Hemolytic Iron Regulation in Traumatic Brain Injury and Alcohol Use

Agnieszka Agas (ama59@njit.edu)
New Jersey Institute of Technology https://orcid.org/0000-0001-8564-3168
Arun Reddy Ravula
New Jersey Institute of Technology
Xiaotang Ma
New Jersey Institute of Technology
Yiming Cheng
New Jersey Institute of Technology
Kevin D. Belfield
New Jersey Institute of Technology
James Haorah
New Jersey Institute of Technology

Research Article

Keywords: alcohol, TBI, hemorrhage, iron, microglia

Posted Date: October 22nd, 2021

DOI: https://doi.org/10.21203/rs.3.rs-991124/v1

Abstract

Hemorrhage is often a major component of traumatic brain injury (TBI). Red blood cells (RBCs) accumulated at the hemorrhagic site undergo hemolysis upon energy depletion. Hemolysis of RBCs is expected to release free iron into the central nervous system (CNS) that must be managed to prevent iron neurotoxicity. Here, we examine the hypothesis that chronic alcohol consumption, as a secondary stressor, may increase iron toxicity in an animal model of TBI by altering the iron management pathways. To our best knowledge, this innovative idea with significant scientific premises has not been examined to date. We found huge accumulation of free irons at the site of hemorrhage with evidence of hemolytic activity. Our observation showed that alcohol use altered the three distinct iron management pathways of transferrin/hemosiderin binding, lipocalin 2/heme oxygenase 1/ferritin system, and microglial phagocytosis. Presence of alcohol prolonged the expression of lipocalin 2 at the site of hemorrhage compared with injury alone, while the combined effects of alcohol and TBI elevated the levels of heme oxygenase 1 earlier than TBI alone. Hippocampus, neocortex, and around vessels near the site of impact appeared to be the prominent brain regions of induction. The presence of alcohol notably increased the levels of ferritin that sustained for up to 7 days. We also provide evidence that microglia also play a role in iron management through RBC phagocytosis. These results reveal the intricacy and plasticity of iron management and highlight the importance of proper iron regulation in the CNS.

Highlights

- Chronic alcohol exposure increases hemorrhage and RBC accumulation following FPI.
- Alcohol alters iron regulatory patterns by shifting LCN2, HO-1, and F-LC expressions.
- Activated microglia can regulate iron accumulation by phagocytosing RBCs.

1. Introduction

Traumatic brain injury (TBI) is a form of injury to the brain caused by an external force and can lead to brain dysfunction. Various animal models of TBI such as blast, weight-drop, and fluid percussion have observed inflammation, edema, oxidative stress, and blood-brain barrier breach after the insult corresponding to behavioral deficits [1–4]. One of the major pathological even of TBI is intracranial bleeding and subsequent cerebral hemorrhage such as epidural/subdural, subarachnoid, intraventricular, and hematoma [5, 6]. These intracranial hemorrhages are constantly being detected in TBI patients by fast magnetic resonance imaging and computerized tomography scanning [7]. Interestingly, these hemorrhages are observed in conjunction with anemia and coagulopathy, therefore current treatment practices include anticoagulant or red blood cell (RBC) transfusion [8, 9]. However, these therapies do not improve neurological function, in fact, RBC transfusions have been shown to significantly exacerbate trauma complications [10]. Since RBCs contain much of the iron found in the body, a possible reason for unresolved, persistent cognitive functional deficits may be neurotoxicity caused by iron overload [11]. We

have observed massive RBC aggregations at the site of hemorrhage in our rat model of blunt TBI [12]. This TBI model uses lateral fluid percussion injury (FPI) delivered at a moderate pressure to reproduce TBI without skull fracturing to generate hemorrhage, subdural hematoma, and edema. FPI causes the rupture of blood vessels through various transient mechanical forces caused by the impact [13]. Even though there are various TBI models, FPI reproducibly recapitulates the pathophysiological signatures of human TBI and thus, can be used to examine the fate of RBC clearance and associated iron release at post-TBI [13].

Accumulated RBCs begin to undergo lysis upon energy depletion (lack of mitochondria) following blood vessel rupture and removal from the circulation at post-TBI [14]. Hemolysis of RBCs releases iron, carbon monoxide, and biliverdin into the central nervous system (CNS) [15]. Destruction of RBCs involves hemolysis and release of RBC constituents, including hemoglobin, heme, and iron, into the extracellular space. Immediately following injury, this released iron is in a free, ferrous (Fe^{2+}) form and can be stained using Turnbull's blue method [16]. Over time, this iron is oxidized to the insoluble ferric (Fe^{3+}) species and can be stained using Prussian blue.

The hemolytic product iron is managed with several different proteins to prevent possible iron toxicity that may develop from iron accumulation. Chief iron regulators include heme oxygenase-1 (HO-1, iron release), lipocalin 2 (LCN2, intracellular iron transport), ferritin light chain (F-LC, iron storage), transferrin (extracellular iron transport), and hemosiderin (iron storage and sequestration) [17, 18]. Heme released from RBCs can trigger the synthesis of HO-1. HO-1 degrades heme by opening its porphyrin ring to release free iron [19]. As the first responding iron managing protein, LCN2 organizes existing iron for chelation, by binding to siderophores, or transport to ensure incoming iron does not accumulate in the cytoplasm. Important to the innate immune response, Currently, LCN2 levels are being used to diagnose several inflammatory diseases [20]. Ferritin, as the primary iron-storage protein of the cell, is paramount to the success of iron management. In fact, ferritin levels are used as a measure to infer iron concentrations in the body [21]. Individuals with hemochromatosis, an inherited mutation in the genes that causes increased iron absorption, show high levels of ferritin while those with anemia, a reduction in RBCs, show low levels and indicate an iron deficiency. Ferritin can partially degrade and combine with lysosomes to create hemosiderin complexes. Together, these proteins combine to form two distinct pathways for iron management, the LCN2/HO-1/F-LC system for intracellular iron and transferrin/hemosiderin binding for extracellular iron. These pathways have been studied following TBI alone, but, to our knowledge, there has been no research on iron management in combined TBI with a secondary stressor such as prior chronic alcohol consumption.

Alcohol use has been shown to prolong neuroinflammation and neurodegeneration at post-TBI by impairing neurological recovery and exacerbating localized neuroinflammation [22, 23]. In addition, as an antiplatelet and anticoagulant, alcohol can thin blood and lead to more profuse bleeding [24]. Chronic alcohol consumption lengthens bleeding times of injured soft tissue by reducing platelet aggregation. Ethanol may interact with platelet cyclooxygenase-1 to inhibit its function and prevent subsequent development of pro-aggregatory proteins. Other hemodynamic changes in blood pressure and vessel

integrity can also contribute to increased bleeding with alcohol. This augmented hemorrhage will result in greater and even faster accumulations of RBCs in the CNS. Together, this suggests that prior alcohol use may increase iron accumulation as well as dysregulate its normal management following TBI. Many studies have already shown that traumatic brain injury activates microglia [25]. Microglia become activated after transitioning through a series of activation states [26]. During this time, microglia undergo changes in both morphology and function. As a result, activated microglia may also play a role in iron management. In this study we examined the time dependent manner of iron regulation by LCN2, HO-1, F-LC, and hemosiderin under combined chronic alcohol exposure and FPI. We also examined whether microglia may be involved in clearing away dying RBCs.

2. Methods And Materials

2.1 Reagents

The OCT compound was purchased from Fisher Healthcare (#4585). Prussian blue soluble was purchased from Santa Cruz (sc-215757), eosin 5% from Sigma (#R03040-74), and hematoxylin solution from Merck (#HX69851575). Primary antibodies were purchased from Santa Cruz, Thermo Fisher, proteintech, and Abcam (**Table 1**). Secondary antibodies were purchased from Thermo Fisher (#32230 and # 32260) for western blots and Abcam (ab64255 and ab97049) for immunohistochemistry. The streptavidin protein was purchased from Abcam (ab7403), Pierce DAB substrate kit from Thermo Fisher (#34002), and Cytoseal XYL from Thermo Scientific (#8312-4). The bicinchoninic acid kit for protein determination was purchased from Thermo Fisher (#23227) and the 4–20% precast protein gel (4561094) and trans-blot PVDF transfer kit (#1704272) were purchased from Bio-Rad. The chemiluminescent substrate was purchased from Advansta (#K-12045-D50).

2.2 Animals

Sprague-Dawley rats were purchased from Charles River Laboratory (Wilmington, MA), they were approximately 8 weeks old and weighed about 240-270 grams at the beginning of the experiment. Rats were kept in reversed 12 hrs. light/dark cycle and housed in controlled temperature and humidity conditions. All experiments were conducted in accordance with the National Institutes of Health institutional ethical guidelines for care of laboratory animals and approved by the Institutional Animal Care Use Committee of Rutgers University (Newark, NJ).

2.3 Alcohol Feeding

Ethanol liquid-diet pair-feeding was employed according to our previously described procedure [27–29]. Briefly, equal pairs of weight-match rats were acclimated to Lieber-DeCarli control or 29% calorie (5% v/v) ethanol liquid-diets (Dyets Inc., Bethlehem, PA) for 1 week followed by pair feeding regimens for 12-14 weeks. Feeding of the control group was based on the amount of ethanol-liquid diet consumed by ethanol group. The control-liquid diet was composed of 47% carbohydrate, 35% fat, and 18% protein while the ethanol-liquid diet was composed of 19% carbohydrate, 35% fat, 18% protein, and 29% ethanol

as percent of total caloric intake. Daily food intake was monitored, and weekly body weights were recorded. By the end of the experiment, the average body weight was 410-420 grams for the control group and 460-490 grams for the ethanol group. Prior to sacrifice, the blood alcohol concentration of all the rats on the ethanol-liquid diet was measured, and it was found to be 9.1-28.8 mM with an average of 15.6 mM which is consistent with our previous findings.

2.4 Fluid Percussion Injury

After alcohol feeding, traumatic brain injury was performed using a fluid percussion injury (FPI) model (Amscien Instruments, Richmond, VA) according to our previously described procedure [12, 30, 31]. Briefly, rats were anesthetized with ketamine (100 mg/kg body weight) and xylazine (10 mg/kg body weight) through intraperitoneal injection and positioned on a stereotaxis frame. Craniotomy was performed by drilling a 3.0 mm size hole on the left parietal skull (2.5 mm lateral of the sagittal suture, 3.0 mm caudal of the coronal suture) leaving the dura intact. A Luer Lock hub was glued to the skull over the exposed dura with cyanoacrylate glue and secured with methyl-methacrylate resin (Henry Schein, Melville, NY). The next day, animals were anesthetized by isoflurane and received lateral FPI. Briefly, the Luer Lock hub of the animal was filled with fluid and fitted into the nozzle of the FPI device. Injury was induced by a pendulum weight striking the piston of a fluid filled cylinder and delivering a fluid pressure pulse to the exposed dura. Severity of the injury was controlled by the position of the weight on the pendulum, all animals received moderate injury or around 2.0 atm pressure [13]. After injury, the hub was removed, the head was sutured, and the rat was returned to it cage. Control animals did not undergo surgery, sham animals underwent surgery but did not receive an injury.

2.5 Tissue Processing

Animals were sacrificed at time points between several hours to 7-days post-injury. Blood samples were collected from the injury site or the carotid artery if no injury was administered and used in western blot analysis. Brains were removed from the skull and thoroughly washed in PBS. Cryopreservation was performed by subsequent overnight incubations in 4% paraformaldehyde, 10% sucrose, and 30% sucrose, respectively. Brains were then snap-frozen in Tissue-Tek OCT compound (Thermo Fisher, Waltham, MA) and stored at 80^{o}C until slicing. Coronal sections (10-20 µm) were cut on a Leica CM3050 cryostat and collected on Fisherbrand Superfrost Plus slides. Slides were air-dried overnight and then stored at -80^{o}C until staining.

2.6 Prussian Blue

This reaction detects ferric iron (Fe^{3+}) in tissue sections. Treatment with acidic solutions of ferrocyanides causes any ferric ions (+3) in the tissue to combine with ferrocyanide and form blue pigments of ferric ferrocyanide. Sections were fixed in ice cold methanol for 10 mins., dried for 20 mins, and rehydrated in PBS for 10 mins. Sections were incubated in a working solution of 5% potassium ferrocyanide with 5% hydrochloric acid for 30 mins. after which they were thoroughly washed in distilled water before being

counterstained with eosin for 1 min. The working solution was prepared fresh every time and discarded after use. Results show iron (hemosiderin) as blue, red blood cells as bright pink, and tissue as light pink.

2.7 Turnbull's Blue

This reaction detects ferrous iron (Fe^{2+}) in tissue. The crystalline structures of Prussian blue and Turnbull's blue compounds are identical but the method by which they are formed is different. Treatment with an acidic solution of potassium ferricyanide causes any ferrous ions (+2) in the tissue to react and form blue pigments of ferrous ferricyanide [16]. Sections were fixed in ice cold methanol for 10 mins., dried for 20 mins, and rehydrated in PBS for 10 mins. Sections were incubated in a working solution of 0.4 mg potassium ferrocyanide with 40 mL 0.006 N hydrochloric acid for 1 hr. after which they were thoroughly washed in 1% acetic acid before being counterstained with eosin for 1 min. The working solution was prepared fresh every time and discarded after use. Results show ferrous iron as blue, red blood cells as bright pink, and tissue as light pink.

2.8 Immunohistochemistry

Prussian and Turnbull's blue were combined with immunohistochemistry in a modified technique previously described by Blomster et., al [32]. Following Prussian or Turnbull's blue staining, sections were incubated with 0.3% H_2O_2 for 10 mins. to quench any endogenous activity. After washing, slides were permeabilized with buffer containing 1% bovine serum albumin and 0.4% Triton X-100 in phosphate buffered saline (PBS) then incubated with 10% bovine serum albumin and 0.4% Triton X-100 in PBS to block non-specific antibody binding. The sections were incubated overnight in a humidified chamber at 4^{o}C with diluted primary antibody: mouse anti-heme oxygenase 1 (1:50, Santa Cruz), rabbit anti-Iba1 (1:200, Abcam), rabbit anti-NGAL (1:500, Thermo Fisher), or rabbit anti-ferritin light chain (1:25, proteintech) (**Table 1**). The following day, slides were thoroughly washed in PBS and incubated with the appropriate secondary antibody, biotinylated goat anti-rabbit (1:500, Abcam) for 1 hr. or biotinylated goat anti-mouse (ready-to-use, Abcam) for 20 mins. After washing, slides were incubated with streptavidin-HRP (1:10,000, Abcam) for 30 mins. After a final washing, staining was developed with 3,3'-diaminobenzidine tetrahydrochloride (DAB, Thermo Fisher) for 20 mins., immersed in distilled water to stop the reaction, and counterstained with eosin for 1 min. Alternatively, slides were counterstained with hematoxylin for 10 mins. and washed in running tap water for 10 mins. Sections were dehydrated through 4, 2 min. changes of alcohol (95%, 95%, 100%, and 100%) and mounted with Cytoseal XYL (Thermo Fisher) solution. Results show stained protein as brown, iron as blue, red blood cells as bright pink, and tissue as light pink. Images were captured with a Leica DMi1 or Aperio Versa 200 microscope and slide scanner.

2.9 Western Blot

Collected blood was centrifuged at 2,100 x g for 10 mins. to separate the plasma for analysis. Protein concentration was estimated using the bicinchoninic acid (BCA) method (Thermo Fisher). 20 µg/lane of protein was loaded into the wells of 4–20% precast polyacrylamide gels (Bio-Rad, Hercules, CA) for

separation. Separated proteins were transferred onto PVDF membranes, blocked with 5% non-fat milk, and incubated at 4^{o}C overnight with the respective antibody (1:1,000 dilution) (**Table 1**). The following day, slides were thoroughly washed in tris-buffered saline with 0.1% Tween 20 and incubated with the appropriate secondary antibody, horse-radish peroxidase conjugated goat anti-mouse or horse-radish peroxidase conjugated goat anti-rabbit for 1 hr. (both 1:10,000, Thermo Fisher). After a final washing, immunoreactive bands were detected with WesternBright ECL chemiluminescent substrate (Advansta). Data was quantified as arbitrary intensity units with densitometry analysis using Image J software.

2.10 Statistical Analysis

Statistical analysis was performed to determine a significant difference in the amount of protein expression between sham and injury. Results were analyzed with independent samples t-tests using the Rcmdr package of R software [33]. Shapiro-Wilk tests were used to validate that the data was normally distributed and Levene's test to check groups did not significantly deviate from variance. Data are presented as mean ± standard error from the mean (SEM). The threshold for statistical significance was $p \leq 0.05$ ($* \; p \leq 0.05$, $** \; p \leq 0.01$ and $*** \; p \leq 0.001$).

3. Results

3.1 FPI indirectly causes iron accumulation in the CNS.

Prussian and Turnbull's blue methods were sensitive enough to stain for iron produced by just one RBC (**Fig. 1**). In addition, both Prussian and Turnbull's blue were able to penetrate cells and stain for iron present inside intact vessels (**Fig. 3**) as well as iron trapped by microglia (**Fig. 7**). Finally, these methods did not interfere with other chromogens, such as the naturally occurring bilirubin (**Fig. 1**), however the overlay of multiple stains did cause positive iron to appear different shades of dark blue. Large bleeding in the ventricular systems showed presence of ferrous iron 0-days post-TBI but by 7-days all iron was converted to the ferric form (**Fig. 1**). Understandably, large bleed sites accumulated large deposits of iron while small sites contained considerably less iron. Therefore, the amount of excess iron aggregation depends on the number of RBCs released in hemorrhagic site of TBI.

3.2 Ethanol exposure alters peak LCN2, HO-1, and F-LC expression TBI.

3.2.1 Moderate lateral fluid percussion injury.

transferrin (extracellular iron transport), and hemosiderin (iron storage and sequestration)

We found that the presence of intracellular iron transporter lipocalin 2 (LCN2) was most notable directly at the site of impact, the expression of LCN2 was peaked at 24 hours post-TBI, and returned to Sham levels after 3 days post-injury (**Fig. 2**). Interestingly, LCN2 was found in individual cells throughout the tissue at 24 hours, most significantly in cells surrounding both ruptured and intact vessels. This early expression post-injury is attributable to LCN2 involvement in the innate immune response. The increase in

the levels of heme oxygenase-1 (HO-1) was observed in the hippocampus and neocortex, prominently around the site of impact. The increase in HO-1 level was peaked at day 3 post-injury and it was significantly reduced at day 7 post-injury, which was then found to be localized around the vessels (**Fig. 3**).

The LCN2 and HO-1 are both stress-responsive proteins, as such both the protein levels were expected to significantly increase upon RBC degeneration at day 3 post-injury. Unlike LCN2, Western blot analysis showed significant increase in HO-1 levels ($p<0.001$) compared with sham controls (**Fig. 7.D**). This discrepancy can be explained by LCN2 being primarily localized to the impact site and HO-1 being much more dispersed, and our western blotting was performed on plasma samples leaked out LCN2 or HO-1 protein in the circulatory system. Unlike LCN2 and HO-1, the localization of the iron storage protein ferritin light chain (F-LC) was more perilesional, found in the hypothalamic and basal forebrain regions of the brain. The increase in clusters of F-LC ranging from <1 μm to 50 μm in size was observed time-dependently (1-7 days) post-injury FPI around the RBCs and iron deposits in these areas (**Fig. 4**). This increase in qualitative levels of F-CL ($p<0.001$) compared with sham controls was further validated by quantitative Western blot analysis (**Fig. 7.D**).

3.2.2 Chronic alcohol consumption and FPI.

In the CNS, one result of chronic alcohol consumption was increased presence of LCN2 (**Fig. 2**), HO-1 (**Fig. 3**), and F-LC (**Fig. 4**) when compared to the no alcohol control. As a physiological stressor, ethanol can induce expression of these stress-responsive proteins. Expression was generally ubiquitous for all three proteins, however, some areas along the edge of the neocortex, did show greater expression (**Fig. 4**). The magnitude of expression was also similar for all three proteins. Background staining may be due to low levels of LCN2, HO-1, and F-LC released by cells. We suspect that these iron regulatory proteins may be actively secreted into the exterior of the cell in response to inflammation caused by alcohol presence. However, alcohol consumption dynamically changed the iron management in TBI. LCN2 expression peaked at 24 hours in EtOH + FPI, same as that of FPI alone, but the presence of alcohol prolonged the expression of LCN2 for more than 7-days without altering the location or magnitude of FPI-induced LCN2 (**Fig. 2**). The combined effects of EtOH + FPI was seen to induce HO-1 at 24 hours earlier than with FPI alone (**Fig. 3**). In addition, cellular expression density and intensity appeared greater than that of LCN2. Like FPI, EtOH + FPI-induced HO-1 presence was prominent at the hippocampus, neocortex, and around vessels near the site of impact. The notable combined effects of EtOH + FPI was impacted in the expression F-LC, wherein the increase levels of F-LC peaked at day 3 and sustained these levels up to 7-days (**Fig. 4**).

3.3 Activated microglia are also involved in iron management.

3.3.1 Activation

Sham injuries did not stimulate microglial activation and so microglia appeared resting with dynamic branching of their processes. However, fully activated microglia in round ameboid shapes were observed

as early as 1-day post-FPI. This morphology was sustained at 3-days but by 7-days post-FPI microglia returned to their homeostatic state (**Fig. 6**). In addition, the number of monocyte lineage cells, marked by CD68 expression, also significantly increased compared to sham controls ($p<0.001$) in plasma (**Fig. 7.D**).

Interestingly, we also observed a morphological gradient 3-days post-FPI (**Fig. 7.C**). At the site of blood accumulation, the gathering microglia were in the active ameboid shape but, several micrometers away from this site resident microglia appeared stress-primed with short, thick processes. In this intermediary state, microglia are very reactive and can easily change to any other of the activation states. Microglia furthest away from bleed sites remained in a homeostatic, surveillance-inclined state. Alcohol consumption alone resulted in sustained presence of activated microglia in and around the ventricular systems and inferior colliculus (**Fig. 6**).

In FPI following chronic alcohol exposure, microglia also appeared activated at 1-day, invading cavities near the inferior colliculus. However, unlike in FPI or EtOH alone, there were greater numbers of microglia present (**Fig. 6**). High microglial numbers were sustained 3-days post-EtOH + FPI, but by 7-days, with considerably less RBC presence, there were fewer of these immune cells. However, microglia sustained an activated form 1-, 3-, and 7-days under EtOH + FPI. Under alcohol alone, microglia remained activated for all days, therefore, the addition of FPI only reinforces continuation in this form. Interestingly, several of these microglia also appeared bigger in size. Further investigation revealed that microglia may be phagocytosing moribund RBCs.

3.3.2 Autophagy

At 3-days post-FPI, sites with microglia and RBCs show these microglia ingesting individual, intact RBCs (**Fig. 7.A**). In that same area, a neighboring microglia cell, that has earlier phagocytosed an RBC, was found with free, ferrous iron inside its cell body. The lack of surrounding free iron suggests that this cytoplasmic iron must come from the ingestion and breakdown of an RBC. However, microglia may also be phagocytosing iron-containing complexes seeing as bound, ferric iron was also found in microglia, otherwise, the iron released from ingested RBCs is quick sequestered as hemosiderin (**Fig. 7.B**). With FPI following chronic alcohol consumption at 1-day, microglia appeared more reactive, ingesting more than one RBC or iron-containing complex at a time, and increasing tremendously in size. Conversely, the abundance of RBCs may simply force single microglia to ingest more. Phagocytosis was also observed under EtOH alone at sites with some RBC presence (**Fig. 6**). Low CD68-positive staining confirm that these immune cells were not macrophage.

4. Discussion

4.1 Excess iron is regulated by three distinct pathways.

4.1.1 Hemosiderin and transferrin binding.

Accumulation of red blood cells (RBCs) has been observe in fluid percussion injury (FPI) [34]. These RBCs come from blood vessels ruptured by the transient mechanical forces produced by the impact, in which hemorrhage lasted for several days resulting in a substantial aggregation of RBCs especially in the epidural, subarachnoid, and ventricular spaces [35]. Failure to clear these RBC aggregates may cause the formation of an impacted blood mass and can result in an enduring mass effect. With time RBC aggregates can penetrate neighboring tissue as we observed in our findings (**Fig. 1**). This may be due to their low resistance and viscoelastic properties as previously noted [36]. Interestingly, the most penetration of RBCs was observed at subarachnoid spaces as opposed to any other area. Since the subarachnoid space facilitates fluid flow into the brain, RBCs may be using this current to enter brain tissue [37]. These RBCs homing in tissue cannot survive for long time, they eventually undergo hemolysis to release free irons. We found that iron remains ferrous for only a few hours following injury as ferric iron was observed as early as 1-day post-FPI (**Fig. 4**). This explanation is in agreement with the findings of others [18]. Free iron, whether as a ferrous cation or an unbound ferric species, is readily absorbed by cells and can be very toxic [38]. The unpaired electrons make free iron highly chemically reactive and, through the Fenton-Haber-Weiss reaction, catalyze the formation of free radicals (**Fig. 8**). This may be a reason for iron's rapid transformation from ferrous to ferric, and finally to the bound form by the body.

Although transferrin increased following injury (**Fig. 7.D**), generally, transferrin becomes saturated when ~70% is bound with iron [39]. Western blot analysis showed greater F-LC levels in plasma than transferrin (**Fig. 7.D**). When this main iron binding protein in the blood is so far extended that it cannot bind any more iron, excess catalytic iron must be stored by ferritin or transformed ferritin, i.e., hemosiderin, to prevent iron toxicity. Significant amounts of hemosiderin collections, ranging in size, were found at all bleed sites (**Fig. 7.B**). These results reveal hemosiderin binding as a pathway in iron management specially reserved for superfluous excesses of iron. Iron as hemosiderin is not readily available for release thereby making this binding very stable. Like ferritin binding, iron release from hemosiderin may possibly be achieved by lysosomes (**Fig. 8**). Extracellular hemosiderin complexes may also follow suit and be degraded by strong digestive enzymes. More research is needed on the fate of iron following hemosiderin binding and on understanding the circumstances and elements involved in its release; it is likely lysosomes are involved.

4.1.2 Sequestration by iron regulatory proteins.

Russell et. al. (2019) described a time-dependent induction of the iron regulatory proteins LCN2, HO-1, and F-LC following an FPI-induced traumatic brain injury [18]. We have observed similar results in rats that have undergone FPI alone but a time shift in expression profiles following prior alcohol consumption. In both FPI and EtOH + FPI situations we have observed a similar expression pattern for LCN2 (**Fig. 5**). By immediately trafficking and sequestering iron, LCN2 expression stimulates anticipation for possible incoming or excess iron to prevent its congestion. This result demonstrates that LCN2 induction may not depend on the type of injury but rather by the inflammation associated with the injury. Therefore, if the injury causes any release of inflammatory stimuli, LCN2 becomes expressed. This result demonstrates that combined, alcohol and FPI injuries do not necessarily exacerbate the degree of

inflammation, but rather prolong its persistence. However, failure to resolve this inflammation can lead to a chronic inflammatory state in the CNS and manifest debilitations in attention and cognition [40]. Therefore, by maintaining LCN2 expression, alcohol consumption may transform FPI-induced inflammatory properties. In this way, LCN2 may act as a master switch for the induction of subsequent iron regulatory proteins. LCN2 may occupy a greater role in iron regulation than has been so far suggested.

One important regulator of HO-1 expression is the nuclear transcription factor Nrf2 [41]. Nrf2 also controls production of the antioxidant proteins that protect against the oxidative damage caused by an insult. Therefore, HO-1 is directly related to the presence and extent of oxidative damage. We have previously shown that inflammation, from both FPI and the resulting hemorrhage, can trigger oxidative damage [12]. Since LCN2 expression is determined by inflammation and HO-1 is mediated by oxidative stress, HO-1 induction is expected to occur after LCN2 under FPI (**Fig. 5**). However, alcohol presence causes HO-1 to express concurrent with LCN2 (**Fig. 5**). EtOH + FPI must exacerbate oxidative damage enough to cause this shift to earlier protein expression.

Interestingly, F-LC was observed as clusters. F-LC clustering may be the result of a partial unfolding of the protein shell in preparation for iron binding [42]. Unlike ferritin heavy chain (F-HC), F-LC has no ferroxidase activity, instead it is involved in the transfer of electrons across its protein cage which allows F-LC staining to mark unfolded shells [43]. Notably, we observed a delayed ferritin response following FPI, peaking at 7-days (**Fig. 5**). These results demonstrate that ferritin is the final regulatory protein involved in iron management, sequestering any remaining unbound iron for accessible storage. Even hemosiderin, observed in 1-day post-FPI, precedes significant ferritin expression (**Fig. 4**). Furthermore, this delay shows ferritin to be induced primarily by iron release and secondarily by heme presence. Low ferritin levels under EtOH alone suggest that ferritin is nominally induced by stress. However, EtOH + FPI caused early, increased, and sustained ferritin expression. Due to the excess RBC accumulation following these combined injuries, much of this ferritin may be being excreted and transformed to hemosiderin for more stable storage. These increased ferritin levels also imply high iron concentrations in the CNS.

4.1.3 IRPs also function in the extracellular space.

Interestingly, LCN2, HO-1, and F-LC were also expressed directly atop bleed sites, interacting with RBCs (**Fig. 4**). This presence may be explained by the mechanical forces caused by the impact bursting cells and releasing intracellular proteins into the extracellular space. As demonstrated, alcohol may also help facilitate secretion of these proteins by increasing their basal levels. There is evidence of LCN2, HO-1, and F-LC secretion in other organ systems. Hepatic cells have been shown to secrete ferritin, while HO-1 has been found in various extracellular, fluid filled compartments and LCN2, as a mediator of inflammation, is routinely released by various cell types, most notably immune cells [44-46]. Extrapolating these findings and relating then to the CNS space, HO-1 may be in the CSF while LCN2 gets secreted by astrocytes and microglia, and ferritin released by neurons. Then protein targeting mechanisms may explain their localization at sites of RBC aggregation. More research on the default expression levels and

locations of LCN2, HO-1, and F-LC in the CNS as well as their intrinsic signaling sequences help explain this phenomenon.

LCN2/HO-1 colocalization can indicate that even HO-1 may not be constrained to expression following FPI, instead it can be induced by the oxidative stress accompanying inflammation [47]. Meanwhile, LCN2/F-LC colocalization suggests LCN2 expression may recruit F-LC generation in preparation for iron sequestration. The lack of microglial expression of these iron regulatory proteins suggests microglia may not be involved in the lipocalin 2/heme oxygenase 1/ferritin system of iron management. Another limitation of this study was confining it to 7-days. However, previous studies have shown that beyond 7-days, LCN2, HO-1, and F-LC levels comparatively return, or being to return, to basal levels in most cells of the CNS [18]. A notable exception are microglia which have shown elevated HO-1 expression as late as 30-days relative to controls under a moderate cortical impact [48]. In this effect, we argue that microglial involvement may create a separate pathway for iron management, removed from that created by the iron regulatory proteins of the remaining CNS cells.

4.1.4 Microglial phagocytosis.

To our knowledge, this is the first demonstration of RBC phagocytosis by microglia and subsequent cytosolic iron deposition following injury. Previous studies revealing iron presence in microglia have only considered this accumulation as iron retention and a signature of microglial activation [49]. The idea of a link between iron management, by extent metabolism, and activated microglia has been contemplated for some time [50]. Moreover, the capacity for RBC autophagy by microglial cells has already been well established as an important corrective response to CNS hemorrhage [51]. In agreement with previous studies, we have observed microglial activation following FPI alone in the present work, as well as following chronic alcohol exposure [52, 53]. Interestingly, many of these activated microglia remained in the tissue at 1-day, only being present around RBCs and bleed sites 3-days post-FPI. These results demonstrate that morphology precedes function and, although reacting quickly to an injury, microglia may have a delayed immune response to invading RBCs. However, microglia may be responding to only atypical RBCs such as those dying from nutrient deprivation after being confined in tissue for 3-days post-FPI.

Other studies as well as our own also observed ethanol induced microglial activation [26, 54-56]. Expectedly, the combination likewise caused microglia activation and greater numbers to gather at sites with RBC aggregation (**Fig. 7.B**). Chronic alcohol use prior to FPI may be sensitizing microglia to stress and, in this manner, preconditioning the brain to future injuries. In other words, the CNS stays in ‘high alert’ for possible stress so that when stress does appear an appropriate response is rapidly mobilized. This state of hypervigilance may dysregulate inflammatory and immune responses to cause inappropriate and even exaggerated reactions. In this respect we observed multiple RBCs within activated microglia following EtOH + FPI. This excessive phagocytosis may either be due to chronic phagocytic activity or the engulfment of multiple RBCs at once. Similarly, the increased number of microglia present may either be the result of migration, division, or a degree of both. Our future work will include studies

exploring these fundamental possibilities. A recent study has shown that microglia can assume a range of phenotypes under alcohol dependency and much remains to be understood in regard to their activation [57].

Collectively, these results begin to distinguish a pathway for iron maintenance by microglial cells. Activated microglia phagocytose and hemolyze RBCs, catabolize heme, and release free iron. Immediately, this iron gets bound to ferritin or hemosiderin. Any extracellular free iron becomes bound to apotransferrin or hemosiderin to form iron-containing complexes. Knowledge of macrophage iron management can be used to infer other details of the microglial-centric pathway. One role of macrophage is to phagocytose senescent RBCs [58]. Therefore, in behaving like macrophage, activated microglia have been observed to also phagocytose RBC aggregations and, in so doing, regulate excess iron presence in the CNS. Heme transporters may also be involved in transporting heme into the cell or release it from plasma membrane-derived vacuoles following phagocytosis. Increases in the labile iron pool may cause excess iron to catalyze production of reactive oxygen species. Iron release may be inhibited by hepcidin hormone binding to and degrading ferroportin transporters. As iron can only bind when in the ferric form, membrane bound ferroxidases may be oxidizing the ferrous form. As an additional idea, the debris following RBC hemolysis and heme release may be shuffled to lysosomes for degradation (**Fig. 8**). Any lysosomal iron may be combined with partially degraded ferritin protein to create hemosiderin. Finally, additional stressors may free iron and evoke toxicity such as ferroptosis, an iron-dependent programmed cell death [59]. Many directions remain to be studied in an effort to understand iron management by microglial cells. We have only begun to discover this alternative pathway of iron regulation.

4.2 Alcohol's influence extends to iron management.

Being soluble in water, alcohol distributes into fluid spaces, as a result, higher concentrations of ethanol can be found in blood, or cerebral spinal fluid (CSF) surround the brain [60]. As the major alcohol filtrating and metabolizing organ of the body, the liver becomes an obvious site for alcohol-induced iron build-up [61]. In fact, this iron accumulation has been shown to contribute to the onset of alcoholic liver disease. This then develops into hepatitis and, over time, liver cirrhosis and destruction. In these same respects, generation of iron deposits in the brain may also lead to a form of inflammation and, if not corrected, neurodegeneration. We have shown that alcohol consumption increases bleeding and consequent iron deposition in the CNS (**Fig. 7.B**). In addition, alcohol abuse has also been shown to frequent rebleeding incidents and, in so doing, can augment deposition numbers even more [62]. Despite this, we did not observe noticeable amounts of ferrous iron under EtOH + FPI. Therefore, although alcohol consumption significantly increases iron load in the CNS, the iron regulatory mechanisms adapt to accommodate this upsurge and prevent free iron accumulation and iron toxicity. To this effect, we have shown that prior chronic alcohol exposure changes the response of all three iron management pathways following FPI (**Fig. 5**). It may be that continued chronic alcohol consumption following FPI is required to release hemosiderin bound iron. This persistent stress would prevent inflammation from resolving and deregulate CNS functions. One affected system may be iron storage wherein the hemosiderin protein

complex becomes destabilized and releases iron. Our future research will examine iron aggregation and regulation when chronic alcohol consumption is continued following FPI (an EtOH + FPI + ETOH model).

5. Conclusion

The iron management system in the body is very efficient, especially so in the CNS. This becomes most evident when examining iron regulation under FPI following chronic alcohol consumption. In effect, three distinct pathways coordinate to ensure iron is only ever briefly unbound. The LCN2/HO-1/F-LC arrangement serves to identify, extract, and sort excess iron coming from its primary source, hemorrhage. Meanwhile, transferrin and hemosiderin binding control the overflow. We have shown that microglia play a role as well in clearing away some RBCs and iron deposits. Even with these processes, the CNS has additional chelators and neuromelanin to trap more iron. There may also be even more iron regulatory pathways and iron toxicity safeguards yet to be discovered. These results contribute to and expound upon the impressive iron management system.

Declarations

Ethics Approval

Not applicable

Consent to participate

Not applicable

Consent for publication

Not applicable

Availability of data and materials

The datasets generated during and/or analyzed during the current study are available from the corresponding author on reasonable request.

Competing interests

The authors declare that they have no competing interests.

Funding

This work was supported by a grant from the NIH/NIAAA (#5R21AA028340-02) awarded to JH.

Authors' contributions

AA carried out the studies, acquired the data, and was involved with preparing the manuscript. AR acquired the images and helped AA analyze data. XM and YC conducted the alcohol feeding and performed the fluid percussion injury. KB proofread the manuscript and provided important comments. JH design the project and was involved with preparing the manuscript. All authors read and approved the final manuscript.

Acknowledgments

This work was supported by a grant from the NIH/NIAAA (#5R21AA028340-02) awarded to JH.

Authors' statement

All authors certify that they have participated sufficiently in the work to take responsibility for the content. Each author certifies that this material has not been previously published or submitted for publication elsewhere.

Compliance with Ethical Standards

Disclosure of potential conflicts of interest

The authors declare that they have no potential conflicts of interest.

Research involving Human Participants and/or Animals

All experiments were conducted in accordance with the National Institutes of Health institutional ethical guidelines for care of laboratory animals and approved by the Institutional Animal Care Use Committee of Rutgers University (Newark, NJ).

Informed Consent

Not applicable

References

1. Aravind A, Ravula AR, Chandra N, Pfister BJ, *Behavioral Deficits in Animal Models of Blast Traumatic Brain Injury*. Frontiers in Neurology, 2020. 11(990)
2. Kuriakose M, Younger D, Ravula AR, Alay E, Rama Rao KV, Chandra N (2019) Synergistic Role of Oxidative Stress and Blood-Brain Barrier Permeability as Injury Mechanisms in the Acute Pathophysiology of Blast-induced Neurotrauma. Sci Rep 9(1):7717
3. Nyanzu M, Siaw-Debrah F, Ni H, Xu Z, Wang H, Lin X, Zhuge Q, Huang L (2017) Improving on Laboratory Traumatic Brain Injury Models to Achieve Better Results. Int J Med Sci 14(5):494–505
4. Rana P, Rama Rao KV, Ravula A, Trivedi R, D'Souza M, Singh AK, Gupta RK, Chandra N (2020) Oxidative stress contributes to cerebral metabolomic profile changes in animal model of blast-

induced traumatic brain injury. Metabolomics 16(3):39

5. Lee JJ, Segar DJ, Morrison JF, Mangham WM, Lee S, Asaad WF (2018) Subdural hematoma as a major determinant of short-term outcomes in traumatic brain injury. J Neurosurg 128(1):236–249
6. Perel P, Roberts I, Bouamra O, Woodford M, Mooney J, Lecky F (2009) Intracranial bleeding in patients with traumatic brain injury: A prognostic study. BMC Emerg Med 9(1):15
7. Schweitzer AD, Niogi SN, Whitlow CT, Tsiouris AJ (2019) *Traumatic Brain Injury: Imaging Patterns Complications* RadioGraphics 39(6):1571–1595
8. East JM, Viau-Lapointe J, McCredie VA (2018) Transfusion practices in traumatic brain injury. Curr Opin Anaesthesiol 31(2):219–226
9. Stolla M, Zhang F, Meyer MR, Zhang J, Dong J-F (2019) *Current state of transfusion in traumatic brain injury associated coagulopathy* Transfusion 59(S2):1522–1528
10. Salim A, Hadjizacharia P, DuBose J, Brown C, Inaba K, Chan L, Margulies DR (2008) Role of anemia in traumatic brain injury. J Am Coll Surg 207(3):398–406
11. Daglas M, Adlard PA (2018) The Involvement of Iron in Traumatic Brain Injury and Neurodegenerative Disease. Front Neurosci 12:981
12. Ma X, Cheng Y, Garcia R, Haorah J (2020) Hemorrhage Associated Mechanisms of Neuroinflammation in Experimental Traumatic Brain Injury. J Neuroimmune Pharmacol 15(2):181–195
13. Ma X, Aravind A, Pfister BJ, Chandra N, Haorah J (2019) Animal Models of Traumatic Brain Injury and Assessment of Injury Severity. Mol Neurobiol 56(8):5332–5345
14. Magnani M, Stocchi V, Cucchiarini L, Chiarantini L, Fornaini G (1986) Red blood cell phagocytosis and lysis following oxidative damage by phenylhydrazine. Cell Biochem Funct 4(4):263–269
15. Wimmer I, Scharler C, Kadowaki T, Hillebrand S, Scheiber-Mojdehkar B, Ueda S, Bradl M, Berger T, Lassmann H, Hametner S (2021) Iron accumulation in the choroid plexus, ependymal cells and CNS parenchyma in a rat strain with low-grade haemolysis of fragile macrocytic red blood cells. Brain Pathol 31(2):333–345
16. Izatt RM, Watt GD, Bartholomew CH, Christensen JJ (1970) Calorimetric study of Prussian blue and Turnbull's blue formation. Inorg Chem 9(9):2019–2021
17. Dev S, Babitt JL (2017) Overview of iron metabolism in health and disease. Hemodial Int 21(S1):S6–S20
18. Russell NH, Black RT, Lee NN, Doperalski AE, Reeves TM, Phillips LL (2019) Time-dependent hemeoxygenase-1, lipocalin-2 and ferritin induction after non-contusion traumatic brain injury. Brain Res 1725:146466
19. Balla J, Vercellotti GM, Nath K, Yachie A, Nagy E, Eaton JW, Balla G (2003) Haem, haem oxygenase and ferritin in vascular endothelial cell injury. Nephrology Dialysis Transplantation 18(suppl_5):v8–v12

20. Abella V, Scotece M, Conde J, Gómez R, Lois A, Pino J, Gómez-Reino JJ, Lago F, Mobasheri A, Gualillo O (2015) The potential of lipocalin-2/NGAL as biomarker for inflammatory and metabolic diseases. Biomarkers 20(8):565–571
21. Timmer TC, de Groot R, Rijnhart JJM, Lakerveld J, Brug J, Perenboom CWM, Baart MA, Prinsze FJ, Zalpuri S, van der Schoot EC, de Kort WLAM (2020) and K. van den Hurk, *Dietary intake of heme iron is associated with ferritin and hemoglobin levels in Dutch blood donors: results from Donor InSight*. Haematologica 105(10):2400–2406
22. Teng SX (2014) M.P., Acute Alcohol Intoxication Prolongs Neuroinflammation without Exacerbating Neurobehavioral Dysfunction following Mild Traumatic Brain Injury. J Neurotrauma 31(4):378–386
23. Lowe PP, Morel C, Ambade A, Iracheta-Vellve A, Kwiatkowski E, Satishchandran A, Furi I, Cho Y, Gyongyosi B, Catalano D, Lefebvre E, Fischer L, Seyedkazemi S, Schafer DP, Szabo G (2020) Chronic alcohol-induced neuroinflammation involves CCR2/5-dependent peripheral macrophage infiltration and microglia alterations. J Neuroinflammation 17(1):296
24. Smith S, Fair K, Goodman A, Watson J, Dodgion C, Schreiber M (2019) Consumption of alcohol leads to platelet inhibition in men. The American Journal of Surgery 217(5):868–872
25. Donat CK, Scott G, Gentleman SM, Sastre M, *Microglial Activation in Traumatic Brain Injury*. Frontiers in Aging Neuroscience, 2017. 9(208)
26. Murugan M, Ravula A, Gandhi A, Vegunta G, Mukkamalla S, Mujib W, Chandra N, *Chemokine signaling mediated monocyte infiltration affects anxiety-like behavior following blast injury.* Brain, Behavior, and Immunity (2020) **88**: p. 340-352
27. Alikunju S, Abdul Muneer PM, Zhang Y, Szlachetka AM, Haorah J, *The inflammatory footprints of alcohol-induced oxidative damage in neurovascular components.* Brain, Behavior, and Immunity (2011) **25**: p. S129-S136
28. Cheng Y, Ma X, Belfield KD, Haorah J (2021) Biphasic Effects of Ethanol Exposure on Waste Metabolites Clearance in the CNS. Molecular Neurobiology
29. Muneer PMA, Alikunju S, Szlachetka AM, Haorah J, *The Mechanisms of Cerebral Vascular Dysfunction and Neuroinflammation by MMP-Mediated Degradation of VEGFR-2 in Alcohol Ingestion.* Arteriosclerosis, Thrombosis, and Biology V (2012) **32**(5): p. 1167-1177
30. Ma X, Agas A, Siddiqui Z, Kim K, Iglesias-Montoro P, Kalluru J, Kumar V, Haorah J (2020) Angiogenic peptide hydrogels for treatment of traumatic brain injury. Bioact Mater 5(1):124–132
31. Sarkar B, Ma X, Agas A, Siddiqui Z, Iglesias-Montoro P, Nguyen PK, Kim KK, Haorah J, Kumar VA (2021) In vivo neuroprotective effect of a self-assembled peptide hydrogel. Chem Eng J 408:127295
32. Blomster LV, Cowin GJ, Kurniawan ND, Ruitenberg MJ (2013) Detection of endogenous iron deposits in the injured mouse spinal cord through high-resolution ex vivo and in vivo MRI. NMR Biomed 26(2):141–150
33. Fox J, B.-V.M., *R Commander.*. 2020
34. Dietrich WD, Alonso O, Busto R, Prado R, Dewanjee S, Dewanjee MK, Ginsberg MD (1996) Widespread hemodynamic depression and focal platelet accumulation after fluid percussion brain injury: a

double-label autoradiographic study in rats. J Cereb Blood Flow Metab 16(3):481–489

35. McKee AC, Daneshvar DH (2015) The neuropathology of traumatic brain injury. Handb Clin Neurol 127:45–66
36. Weisel JW, Litvinov RI (2019) Red blood cells: the forgotten player in hemostasis and thrombosis. J Thromb Haemost 17(2):271–282
37. Cheng Y, Haorah J (2019) How does the brain remove its waste metabolites from within? Int J Physiol Pathophysiol Pharmacol 11(6):238–249
38. Imai T, Iwata S, Hirayama T, Nagasawa H, Nakamura S, Shimazawa M, Hara H (2019) Intracellular Fe(2+) accumulation in endothelial cells and pericytes induces blood-brain barrier dysfunction in secondary brain injury after brain hemorrhage. Sci Rep 9(1):6228
39. Eid R, Arab NT, Greenwood MT (2017) Iron mediated toxicity and programmed cell death: A review and a re-examination of existing paradigms. Biochim Biophys Acta Mol Cell Res 1864(2):399–430
40. Balter LJT, Bosch JA, Aldred S, Drayson MT, Veldhuijzen JJCS, van Zanten S, Higgs JE, Raymond, Mazaheri A (2019) Selective effects of acute low-grade inflammation on human visual attention. NeuroImage 202:116098
41. Kim KW, Yoon CS, Kim YC, Oh H (2019) Desoxo-narchinol A and Narchinol B Isolated from Nardostachys jatamansi Exert Anti-neuroinflammatory Effects by Up-regulating of Nuclear Transcription Factor Erythroid-2-Related Factor 2/Heme Oxygenase-1 Signaling. Neurotox Res 35(1):230–243
42. Shin MK, Kim SI, Kim SJ, Park SY, Hyun YH, Lee Y, Lee KE, Han SS, Jang DP, Kim YB, Cho ZH, So I, Spinks GM (2008) *Controlled magnetic nanofiber hydrogels by clustering ferritin* Langmuir 24(21):12107–12111
43. Arosio P, Elia L, Poli M (2017) Ferritin, cellular iron storage and regulation. IUBMB Life 69(6):414–422
44. Li Volti G, Galvano F, Frigiola A, Guccione S, Di Giacomo C, Forte S, Tringali G, Caruso M, Adekoya OA, Gazzolo D (2010) Potential immunoregulatory role of heme oxygenase-1 in human milk: a combined biochemical and molecular modeling approach. J Nutr Biochem 21(9):865–871
45. Moschen AR, Adolph TE, Gerner RR, Wieser V, Tilg H (2017) Lipocalin-2: A Master Mediator of Intestinal and Metabolic Inflammation. Trends Endocrinol Metab 28(5):388–397
46. Tran TN, Eubanks SK, Schaffer KJ, Zhou CYJ, Linder MC (1997) Secretion of Ferritin by Rat Hepatoma Cells and Its Regulation by Inflammatory Cytokines and Iron. Blood 90(12):4979–4986
47. Jin Z, Kim KE, Shin HJ, Jeong EA, Park KA, Lee JY, An HS, Choi EB, Jeong JH, Kwak W, Roh GS (2020) Hippocampal Lipocalin 2 Is Associated With Neuroinflammation and Iron-Related Oxidative Stress in ob/ob Mice. J Neuropathol Exp Neurol 79(5):530–541
48. Morita A, Jullienne A, Salehi A, Hamer M, Javadi E, Alsarraj Y, Tang J, Zhang JH, Pearce WJ, Obenaus A (2020) Temporal evolution of heme oxygenase-1 expression in reactive astrocytes and microglia in response to traumatic brain injury. Brain Hemorrhages 1(1):65–74

49. McIntosh A, Mela V, Harty C, Minogue AM, Costello DA, Kerskens C, Lynch MA (2019) Iron accumulation in microglia triggers a cascade of events that leads to altered metabolism and compromised function in APP/PS1 mice. Brain Pathol 29(5):606–621
50. Mairuae N, Connor JR, Cheepsunthorn P (2011) Increased cellular iron levels affect matrix metalloproteinase expression and phagocytosis in activated microglia. Neurosci Lett 500(1):36–40
51. Lan X, Han X, Li Q, Yang QW, Wang J (2017) Modulators of microglial activation and polarization after intracerebral haemorrhage. Nat Rev Neurol 13(7):420–433
52. Loane DJ, Kumar A (2016) Microglia in the TBI brain: The good, the bad, and the dysregulated. Exp Neurol 275:316–327
53. Walter TJ, Vetreno RP, Crews FT (2017) Alcohol and Stress Activation of Microglia and Neurons: Brain Regional Effects. Alcohol Clin Exp Res 41(12):2066–2081
54. Fernandez-Lizarbe S, Pascual M, Guerri C (2009) Critical Role of TLR4 Response in the Activation of Microglia Induced by Ethanol. J Immunol 183(7):4733–4744
55. Mishra V, Agas A, Schuetz H, Kalluru J, Haorah J (2020) Alcohol induces programmed death receptor-1 and programmed death-ligand-1 differentially in neuroimmune cells. Alcohol 86:65–74
56. Zhao Y-N, Wang F, Fan Y-X, Ping G-F, Yang J-Y, Wu C-F (2013) Activated microglia are implicated in cognitive deficits, neuronal death, and successful recovery following intermittent ethanol exposure. Behav Brain Res 236:270–282
57. Peng H, Nixon K (2021) Microglia Phenotypes Following the Induction of Alcohol Dependence in Adolescent Rats. Alcohol Clin Exp Res 45(1):105–116
58. Klei TR, Meinderts SM, van den Berg TK, van Bruggen R (2017) From the Cradle to the Grave: The Role of Macrophages in Erythropoiesis and Erythrophagocytosis. Front Immunol 8:73
59. Li J, Cao F, Yin HL, Huang ZJ, Lin ZT, Mao N, Sun B, Wang G, *Ferroptosis: past, present and future.* Cell Death Dis (2020) **11**(2): p. 88
60. Abrahao KP, Salinas AG, Lovinger DM (2017) Alcohol and the Brain: Neuronal Molecular Targets, Synapses, and Circuits. Neuron 96(6):1223–1238
61. Ioannou GN, Dominitz JA, Weiss NS, Heagerty PJ, Kowdley KV (2004) The effect of alcohol consumption on the prevalence of iron overload, iron deficiency, and iron deficiency anemia. Gastroenterology 126(5):1293–1301
62. Kärkkäinen JM, Miilunpohja S, Rantanen T, Koskela JM, Jyrkkä J, Hartikainen J, Paajanen H (2015) Alcohol Abuse Increases Rebleeding Risk and Mortality in Patients with Non-variceal Upper Gastrointestinal Bleeding. Dig Dis Sci 60(12):3707–3715

Tables

Table 1: Source, catalogue number, and dilution factors of antibodies used in immunohistochemistry staining and western blot analyses.

Antibody	Marker for	Species Source	Clonality	Company	Catalog No.	Dilution for IHC	Dilution for WB
Anti-heme oxygenase 1	heme oxygenase 1	mouse	monoclonal	Santa Cruz	sc-390991	1:50	1:1000
Anti-NGAL	lipocalin 2	rabbit	polyclonal	Thermo Fisher	PA5-79590	1:500	1:1000
Anti-ferritin light chain	ferritin light chain	rabbit	polyclonal	proteintech	10727-1-AP	1:25	1:1000
Anti-Iba1	microglia	rabbit	monoclonal	Abcam	ab178847	1:200	-
Anti-CD68	macrophage	mouse	monoclonal	Abcam	ab31630	-	1:1000
Anti-transferrin	transferrin	rabbit	polyclonal	Abcam	ab82411	-	1:1000
Anti-β-actin	beta-actin	mouse	monoclonal	Abcam	ab8226	-	1:1000

Figures

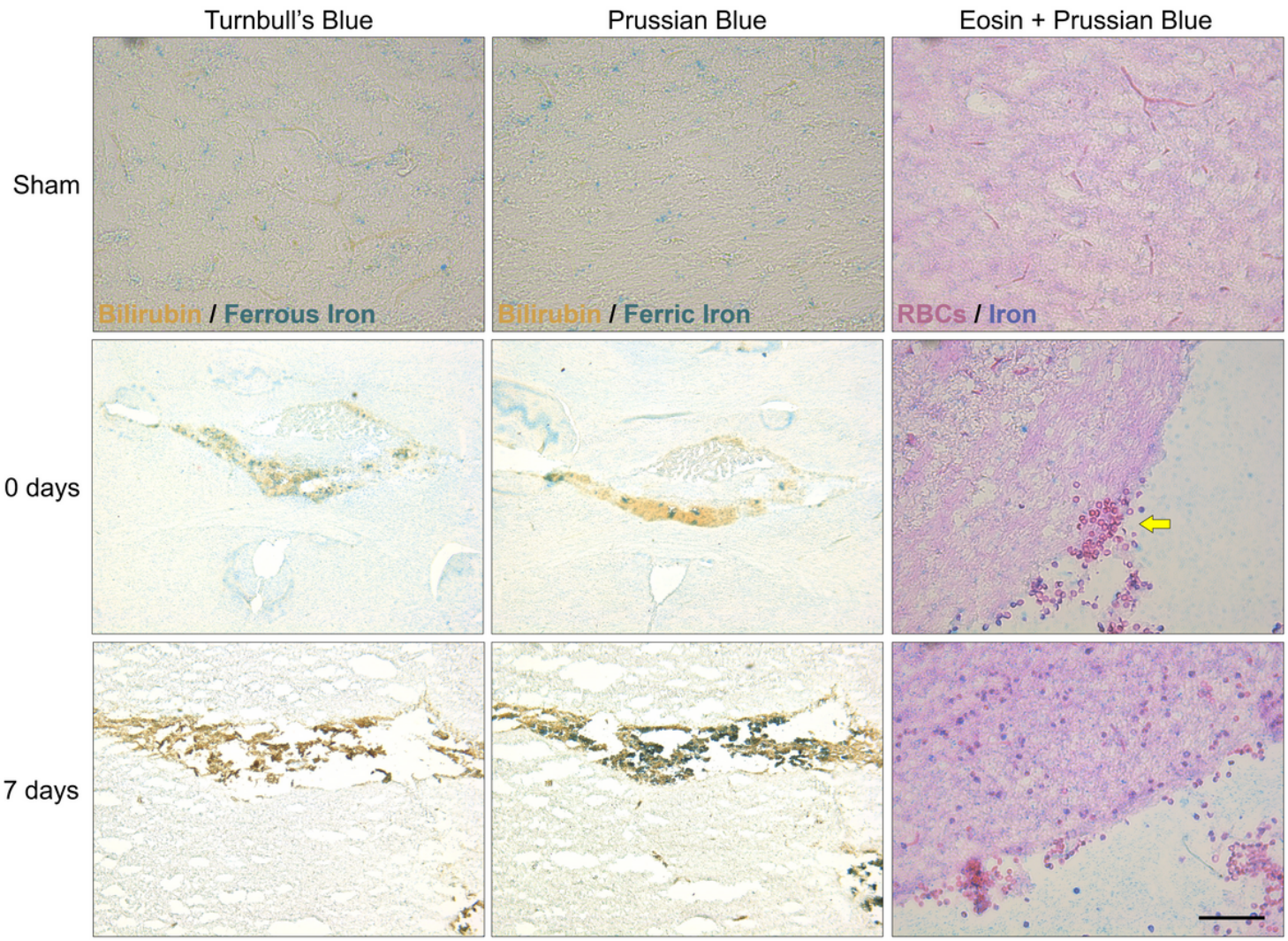

Figure 1

Ferrous and ferric iron expression following FPI. The left and middle column are representative images of presence of both ferrous (Fe+2) and ferric (Fe+3) iron at sham injury (Sham), and 0- and 7-days following moderate fluid percussion injury. Turnbull's blue method stains for free or ferrous iron while Prussian blue stains for ferric iron bound as hemosiderin. Both ferrous and ferric iron are stained dark blue while blood is distinguished by the yellow-brown bilirubin pigment. The right column are representative images of red blood cell penetration into the tissue over time. The yellow arrow points to an accumulation of red blood

cells. Red blood cells are stained dark pink, iron is blue, and tissue is light pink. All images are focused near the ventricular systems or subarachnoid spaces, sites for major blood accumulation post-injury. The black bar represents 100 μm (N = 5 rats).

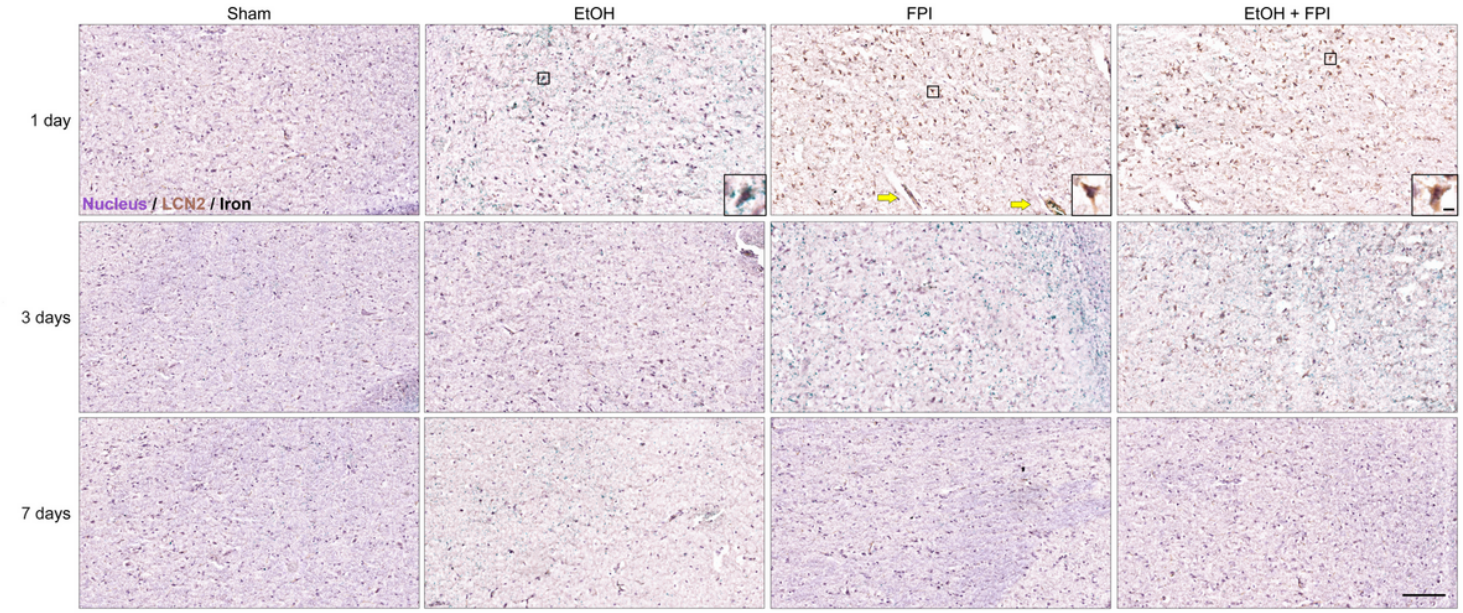

Figure 2

LCN2 induction by alcohol, FPI, and the combination. Representative images of lipocalin 2 expression in rats under sham injury (Sham), ethanol feeding (EtOH), fluid percussion injury (FPI), and injury following ethanol feeding (EtOH + FPI) 1-, 3-, and 7-days post-injury. Images focus on the neocortex at the site of impact. LCN2 is stained brown, nuclei purple, and positive ferric iron staining appears as black. The yellow arrows point to LCN2 expression around both longitudinal and cross-section vessels. The insets are higher magnifications of cells within the black box and demonstrate LCN2 generation by a single cell. The black bar represents 100 μm and inset bar represents 25 μm (N = 5 rats).

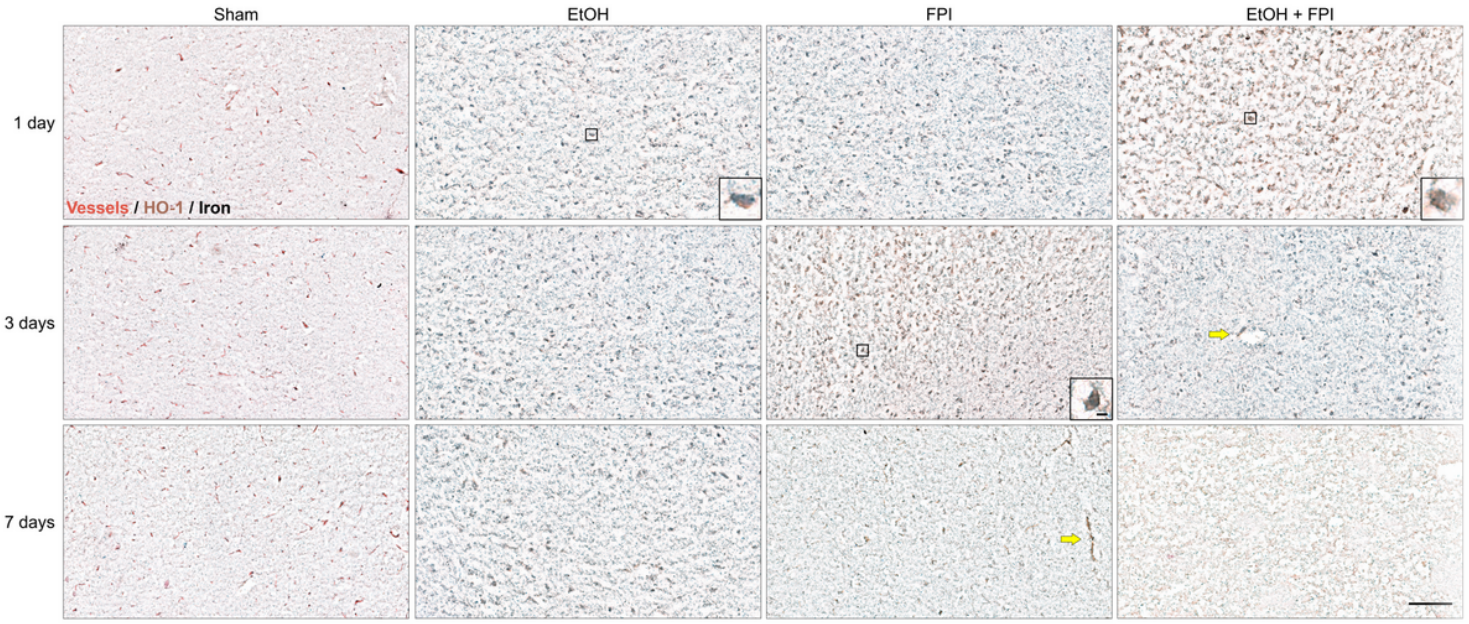

Figure 3

HO-1 induction by alcohol, FPI, and the combination. Representative images of heme oxygenase 1 expression in rats under sham injury (Sham), ethanol feeding (EtOH), fluid percussion injury (FPI), and injury following ethanol feeding (EtOH + FPI) 1-, 3-, and 7-days post-injury. Images focus on the neocortex at the site of impact. HO-1 is stained brown and positive ferric iron staining appears as black. Sham sections also stain for vessels as red. The yellow arrows point to HO-1 expression around both longitudinal and cross-section vessels. The insets are higher magnifications of cells within the black box and demonstrate HO-1 generation by a single cell. The black bar represents 100 μm and inset bar represents 25 μm (N = 5 rats).

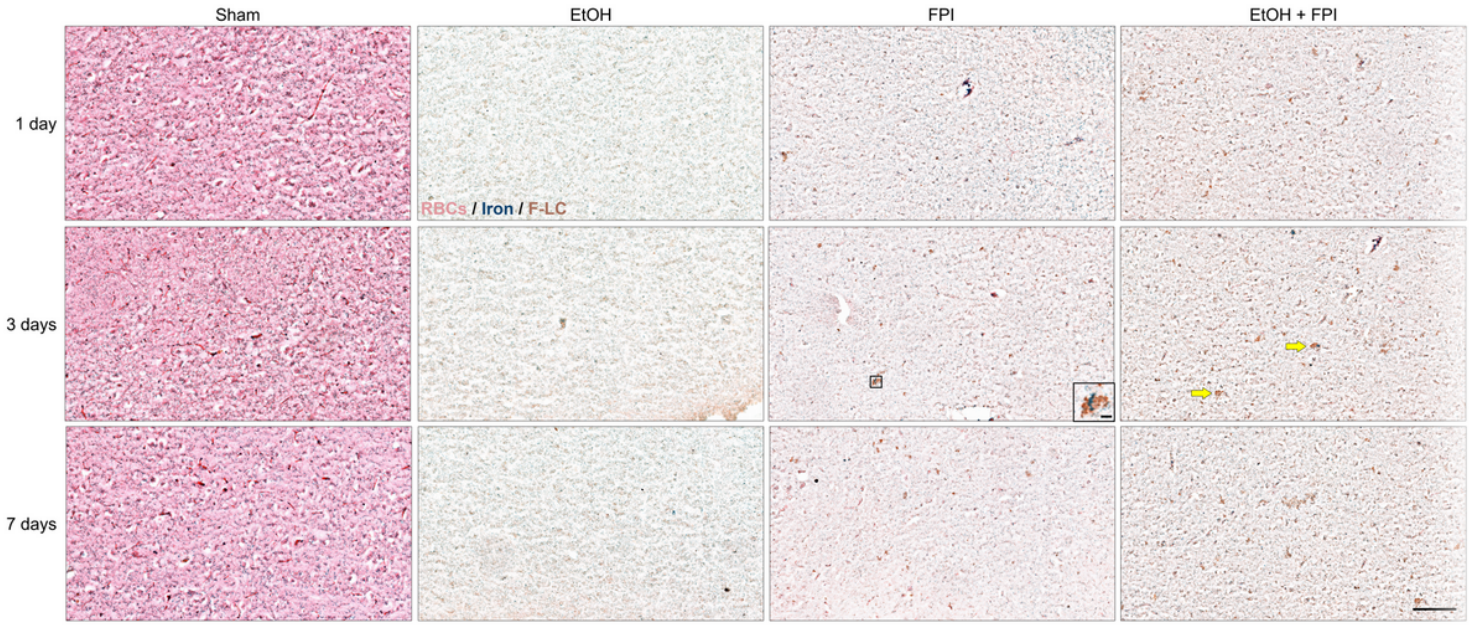

Figure 4

F-LC induction by alcohol, FPI, and the combination. Representative images of ferritin light chain expression in rats under sham injury (Sham), ethanol feeding (EtOH), fluid percussion injury (FPI), and injury following ethanol feeding (EtOH + FPI) 1-, 3-, and 7-days post-injury. Images focus on the hypothalamic and basal forebrain regions. F-LC is stained brown, red blood cells/vessels are red, ferric iron is dark navy, and tissue is light pink. The yellow arrows point to a cluster of F-LC expression. The inset is a higher magnification of cells within the black box and demonstrates F-LC generation at sites of red blood cell and iron accumulation. The black bar represents 100 μm and inset bar represents 25 μm (N = 5 rats).

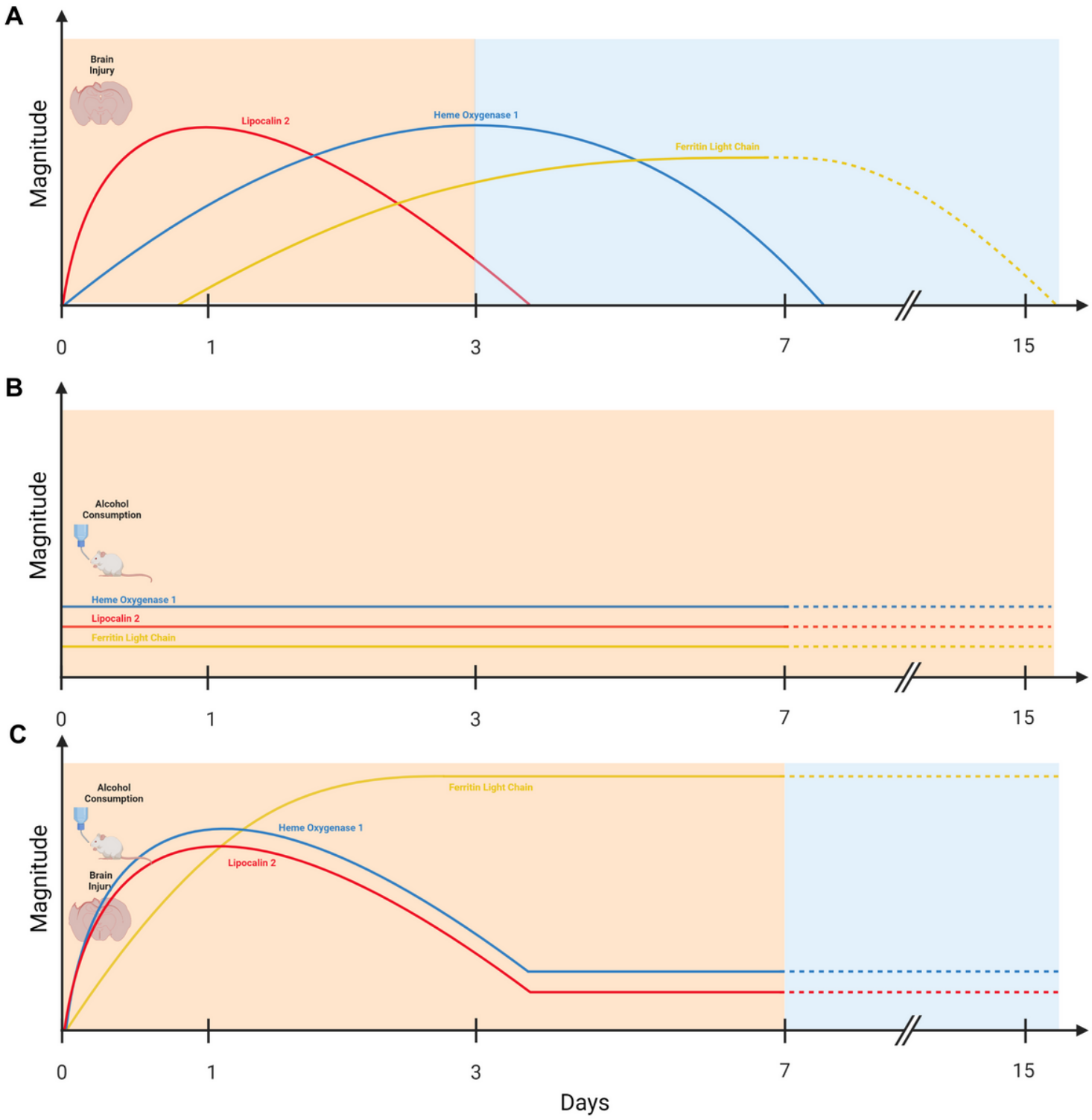

Figure 5

Summary of LCN2, HO-1, and F-LC presence over time. Cartoon graphs depict the expression length and magnitude of each iron regulatory protein after its induction by (A) brain injury, (B) alcohol consumption, or (C) the combination. The magnitude units are arbitrary, time is expressed in days with Day 0 representing injury initiation. The red, blue, and yellow lines denote LNC2, HO-1, and F-LC respectfully. The dashed lines speculate expression after 7-days post-injury. The light orange shading signifies

hemorrhage/a pro-inflammatory response while the light blue shading signifies repair/an anti-inflammatory response. All cartoons were created with BioRender.com.

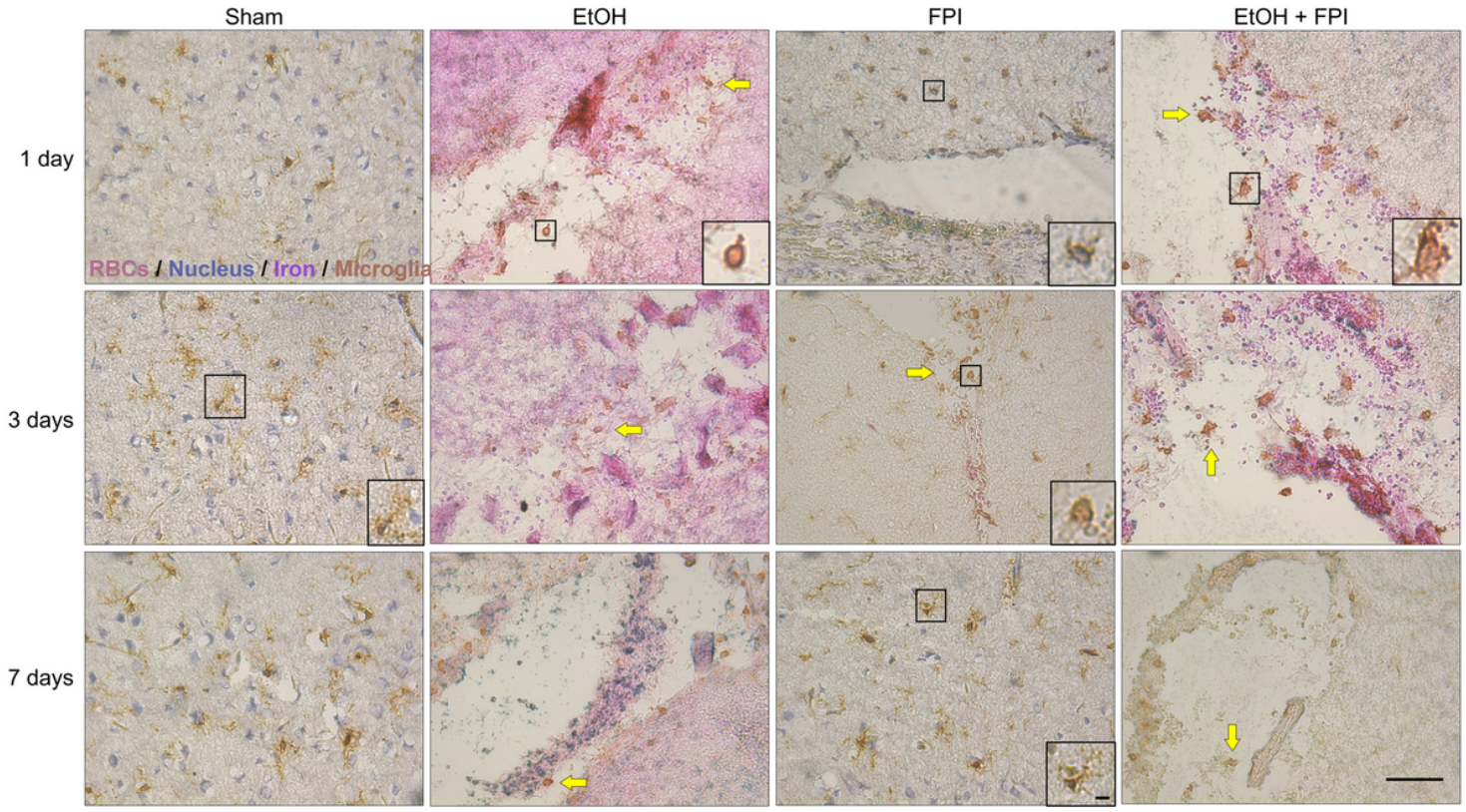

Figure 6

Microglial recruitment and activation by alcohol, FPI, and the combination. Representative images of the microglia-specific calcium-binding protein, Iba1, expression in rats under sham injury (Sham), ethanol feeding (EtOH), fluid percussion injury (FPI), and injury following ethanol feeding (EtOH + FPI) 1-, 3-, and 7-days post-injury. Sham images focus on the neocortex at the site of impact while EtOH, FPI, and EtOH + FPI images are focused near the ventricular systems and inferior colliculus at sites with major blood accumulation. Microglia are stained brown, cell nuclei are blue, red blood cells/vessels are red, ferric iron is purple, and tissue is light pink. The yellow arrows point to microglial recruitment to ventricular cavities and sites of red blood cell accumulation. The insets are higher magnifications of cells within the black box and demonstrate changes in microglial morphology following injury. Homeostatic, resting microglia exhibit dynamic branching while activated microglia take on an amoeboid form. Microglia in transition to the ameboid form have shortener, thicker processes. The black bar represents 100 μm and inset bar represents 25 μm (N = 5 rats).

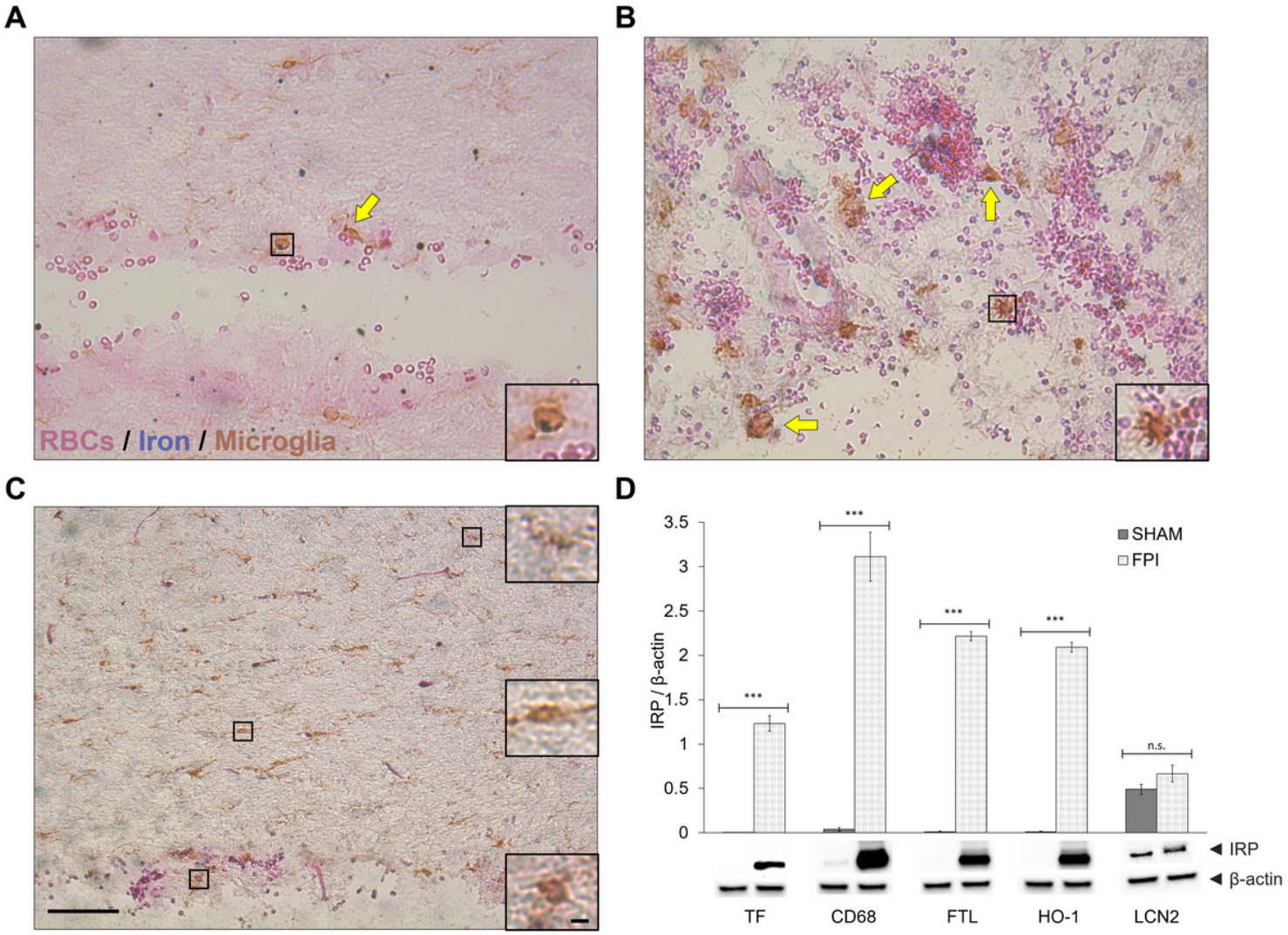

Figure 7

Microglial phagocytosis of accumulated red blood cells. (A) Representative image of microglial phagocytosis of red blood cells near the ventricular systems 3-days post-FPI. The iron stained is in the free, ferrous form. (B) Representative image of microglial phagocytosis of red blood cells in the cavities next to the inferior colliculus 1-day post-EtOH + FPI. The iron stained is in the bound, ferric form. (C) Representative image of a morphological gradient 3-days post-FPI. Microglia next to red blood cells have an ameboid form, those near bleed sites are primed with shorter, thicker processes, and microglia even further away remain in a resting, ramified state. For all images, microglia are stained brown, iron is blue, red blood cells are dark pink, and tissue is light pink. The yellow arrows point to active or completed phagocytosis. The insets are higher magnifications of cells within the black box and demonstrate (A and B) presence of iron and red blood cells inside the microglia or (C) changes in microglial morphology near bleed sites. The black bar represents 100 μm and inset bar represents 25 μm. (D) Bar graph showing western blot analysis of transferrin (TF), monocyte/macrophage marker (CD68), ferritin light chain (FTL), heme oxygenase 1 (HO-1), and lipocalin 2 (LCN2) levels in plasma following sham and FPI injuries. Data were analyzed using ImageJ to obtain arbitrary densitometry intensities and quantified as the ratio of iron regulatory protein (IRP) to β-actin. Results are presented as mean values (±SEM, N = 5 rats). FPI is

compared to Sham injury for each protein. Significant difference is indicated by ∗∗∗ $p \leq 0.001$, n.s. denotes no significance.

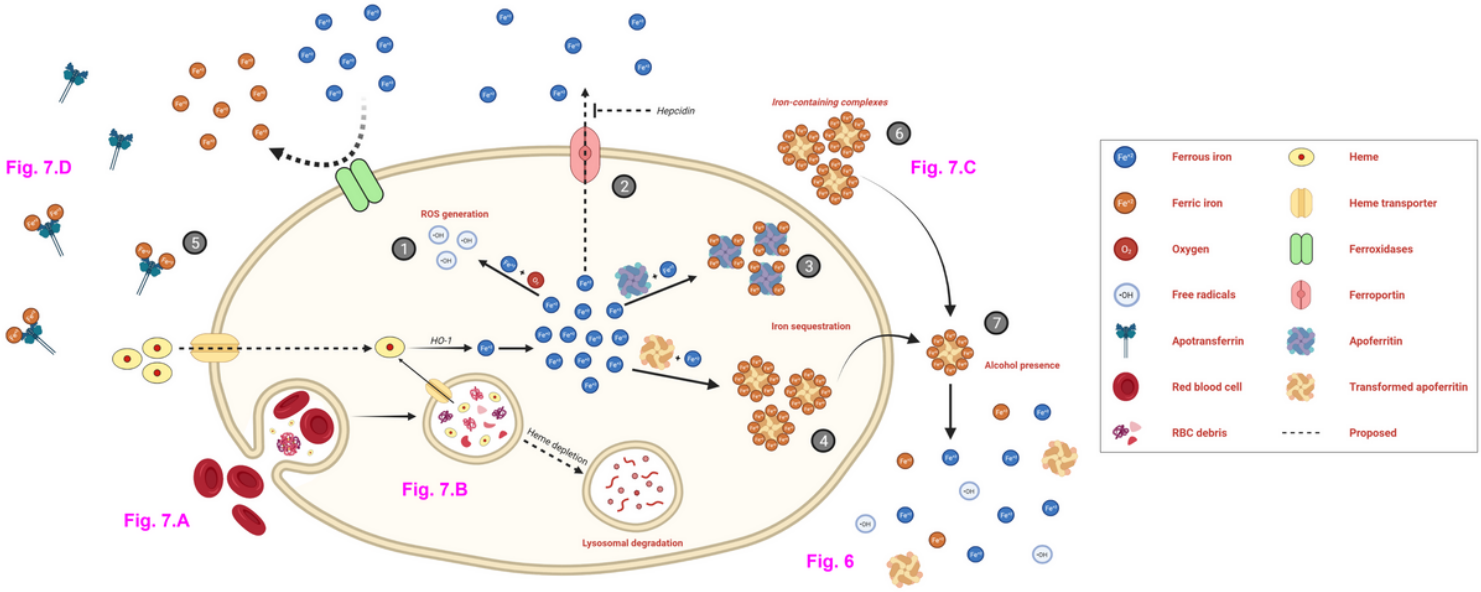

Figure 8

Schematic of iron regulation by activated microglia. Cartoon depicts pathways for microglial management of excess iron following traumatic brain injury. Activated microglia phagocytose red blood cells whereupon heme becomes released. Following heme depletion, any remaining debris may be transported to lysosomes for degradation. Alternatively, extracellular heme may be transferred into the microglia via a heme transporter. Cytosolic heme can be lysed by heme oxygenase 1 to release free iron and increase the labile iron pool. Excessive intracellular iron can be: (1) oxidized to produce reactive oxygen species, (2) released by ferroportin transporters, (3) stored by ferritin, or (4) bound as hemosiderin for long term storage. Excessive extracellular iron can be converted to the more stable, ferric form by ferroxidases and (5) bind to apotransferrin for transportation or, when apotransferin becomes saturated, (6) be stored in iron-containing vesicles. (7) However, in the presence of alcohol, stored iron may be released, converted to its toxic, ferrous form by ferrireductase, and, as a result, generate oxidative stress. The pink text indicates a representative image that depicts this event. The cartoon was created with BioRender.com.